Enhanced Electrochemical Performance of Li₂ZrO₃ coated LiFePO₄ as Cathode Material for Lithium Ion Batteries

Ruitong Guo, Huiting Zhu, Xingyao Wang[*]

Department of Chemistry, School of Sciences, Tianjin University, Tianjin, 300350, China
[*]E-mail: wxyghw@163.com

Li₂ZrO₃-coated LiFePO₄ (LFP@C/LZO) was prepared by hydrothermal synthesis and ex-situ coating for the first time. X-ray diffraction (XRD), scanning electron microscopy (SEM), transmission electron microscopy (TEM), and charge-discharge tests were used to characterize lithium iron phosphate and the influences of different coating amounts on the material were systematically studied. The results show that when Li₂ZrO₃ is 2 wt%, LFP@C/LZO-2 exhibits excellent electrochemical performance where the initial discharge capacities are 156.7 mAh/g and 111 mAh/g at 0.1 C and 1 C, respectively. And after 200 cycles at 1 C, the capacity can retain 81.62% of the initial value. Electrochemical impedance spectroscopy (EIS) shows that the introduction of Li₂ZrO₃ can decrease the charge transfer resistance and improve the lithium-ion diffusion rate. The study reveals a moderate amount of Li₂ZrO₃ can helpfully enhance the electrochemical properties of LFP and broadens options for surface coating of LFP and other electrode materials.

1. INTRODUCTION

Lithium iron phosphate has received much attention because of its low cost, environment friendly, superior structure stability, and long cycle life [1-3]. However, two drawbacks, which are low electronic conductivity and sluggish ion diffusivity, both limited their practical use in power batteries. To solve this problem, many works have been done including particle size reduction [4,5], foreign ion doping [6-12], conductive layer coating [13-16] and so on. Carbon coating is recognized as the most effective means to improve the electrochemical properties of lithium iron phosphate. It can not only improve the electronic conductivity [17], but also inhibit the growth and agglomeration of lithium iron phosphate during sintering. It can also increase the specific surface area of the material and enhance the contact between the electrolyte and the electrode material. Unfortunately, the excess introduction of carbon also reduces the tap density of the material [18] and introduces other impurity phases [19], which

has a detrimental effect on increasing the energy density. Therefore, it is an urgent problem to seek a coating material that can improve the electrochemical performance of the material without compromising the tap density of the material and form a lithium-ion transport channel on the surface.

Ionic conductors are regarded as ideal coating materials to improve high-rate performance due to their favorable characteristics for the transport of lithium ions at the interface between the cathode material and the electrolyte. Zhao and Ding [20] reported that Li_3PO_4 coating can enhance the rate performance and help decrease interface resistance. Zhao et al [21] adopted Si-doping and carbon and Li_2SiO_3 hybrid-coating to enhance the rate performance of $LiFePO_4$ (LFP). Among them, Li_2SiO_3 can not only enhance the diffusion rate of lithium ions, but also reduce the corrosion of the electrolyte to the cathode material. Besides, $CePO_4$ [22], $Li_{1.4}Al_{0.4}Ti_{1.6}(PO_4)_3$ [23], $LaPO_4$ [24] and $Na_3V_2(PO_4)_3$ [25] ionic conductors are also used in the modification of LFP, and these results also fully demonstrate that ionic conductors have a significant effect on improving electrochemical performance and enhancing material stability. Li_2ZrO_3 (LZO) is a common lithium-ion conductor with a three-dimensional channel for lithium-ion diffusion and high thermal stability [26]. It has been successfully used as a surface coating material to improve the lithium-ion diffusion rate and rate performance of many cathode materials, such as $LiCoO_2$ [27], $Li_4Ti_5O_{12}$ [28], $LiNi_{0.5}Co_{0.2}Mn_{0.3}O_2$ [29], $Li_3V_2(PO_4)_3$ [30], etc. However, there are few studies on the influence of LZO on LFP cathode materials.

In this study, we used the hydrothermal method to synthesize lithium iron phosphate and carried out an ex-situ coating of LZO and carbon on its surface. In this case, carbon can improve its electronic conductivity, and LZO acts as an ionic conductor to speed up the transport of lithium ions between the electrolyte and the bulk material. Such a co-coating structure greatly avoids the inherent defects of LFP cathode materials and is an efficient and simple method for the improvement of the electrochemical performance of materials. The influences of the content of LZO on its phase structure, morphology and electrochemical performance were disclosed. The results show that the small content of LZO coating is beneficial to improve its electrochemical performance.

2. EXPERIMENTAL

2.1 Synthesis of LFP@C

The LFP@C was synthesized using the conventional hydrothermal method. LiOH (AR, Tianjin Jiangtian Chemical Technology Co., Ltd), H_3PO_4 (85 wt%, Tianjin Fengchuan Chemical Reagent Technology Co., Ltd) and $FeSO_4 \cdot 7H_2O$ (AR, Tianjin Damao Chemical Reagent Factory) were dissolved in deionized water with a molar ratio of 3:1:1, in which iron concentration was 0.4 mol/L. A certain amount of ascorbic acid (AR, Fuchen Chemical Reagent Co., Ltd) was used to protect Fe^{2+} from oxidation. The solution was vigorously stirred and then poured into an autoclave with a volume of 100 mL, and heated at 220°C for 4 h. After cooling, the obtained precursor was rinsed with deionized water, centrifuged, and vacuum dried at 80°C. Then, the LFP was mixed uniformly with 25 wt% glucose (AR, Tianjin Damao Chemical Reagent Factory) and kept at 650°C for 6 h under the protection of Ar

(99.999%, Tianjin Liufang Industrial Gas Distribution Co., Ltd). After cooling, the resulting black powder is carbon-coated lithium iron phosphate (LFP@C).

2.2 Synthesis of LZO coated LFP@C

The sol-gel method was used to synthesize LZO, the process was as follows [30]: 0.02 mol CH_3COOLi (99.9%, Aladdin) and 0.01 mol $Zr(NO_3)_4 \cdot 5H_2O$ (AR, Tianjin Comeo Chemical Reagent Co., Ltd) were respectively dispersed in 50 mL of absolute ethanol (AR, Tianjin Jiangtian Chemical Technology Co., Ltd). Then we dropped the CH_3COOLi solution into the $Zr(NO_3)_4 \cdot 5H_2O$ solution dropwise and set the heating temperature to 80°C. Keep stirring until a white sticky substance appeared. The substance was dried at 100 °C for 8 h to remove excess ethanol and subsequently calcined at 700°C for 5 h in the air. The white powder obtained is Li_2ZrO_3.

In order to obtain Li_2ZrO_3-coated $LiFePO_4$ (LFP@C/LZO), different amounts of LZO (0.01 g, 0.02 g, 0.04 g) were weighed and dispersed in 20 mL of absolute ethanol, and then 1 g of LFP@C was slowly poured into it. The mixed solution was constantly agitated at 80°C until solid appeared and subsequently vacuum dried at 80°C to get LFP@C/LZO. The samples coated with 0.01 g, 0.02 g, and 0.04 g LZO are named LFP@C/LZO-1, LFP@C/LZO-2, LFP@C/LZO-4, respectively.

2.3 Structural Characterization

The phase structure of the sample was investigated by X-ray diffraction (XRD, D8-Focus) in the range of 10-60° with a scanning rate of 8°/min. The morphology and carbon layer of the samples were detected by a scanning electron microscope (SEM, Apreo S LoVac) equipped with energy dispersion spectroscopy (EDS) mapping and transmission electron microscope (TEM, JEOL-2100F). Thermogravimetric analysis (TG) was tested on a thermogravimetric analyzer (TG, Q50) with a temperature range of 40-700°C and a heating rate of 10°C /min.
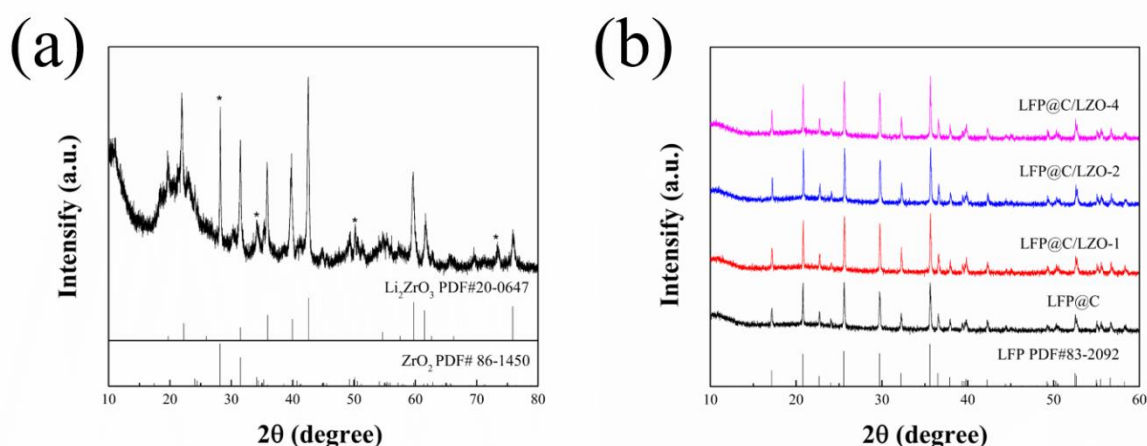
2.4 Electrochemical Measurement

For the fabrication of electrodes, we weighted cathode material, acetylene black, polyvinylidene fluoride (PVDF) with a mass ratio is 8:1:1. N-methyl-2-pyrrolidone (NMP) was added dropwise until a sludge was formed and stirred for 12 h in a sealed environment. Afterward, the sludge was evenly coated on aluminum foil and dried at 80°C. Then we cut the aluminum foil into 14 mm discs and vacuum dried it at 120°C for 12 h. Finally, the C2032 battery was fabricated in an argon glove box. Lithium metal and Celgard 2400 were used as the counter electrode and the separator, respectively. The electrolyte was 1.0 M $LiPF_6$ dissolved in a mixed solvent of ethylene carbonate (EC), dimethyl carbonate (DMC), and ethylmethyl carbonate (EMC).

Cyclic voltammetry (CV) curves were measured by electrochemical analyzer CHI604C at a voltage range of 2.5-4.2 V and a scan rate of 0.1 mV/s. Electrochemical impedance spectroscopy (EIS)

measurements were conducted with the frequency ranges of 100 kHz to 10 mHz. The charge-discharge tests were carried out on a Land CT2001A system at a voltage of 2.5-4.2 V at room temperature.
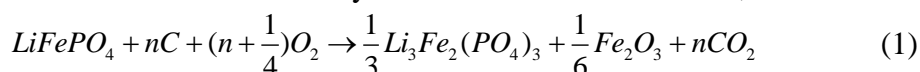
3. RESULTS AND DISCUSSION

Figure 1a is the XRD patterns of the as-prepared LZO. It can be found that the main diffraction peaks of the sample can well correspond to LZO (JCPDs PDF# 20-0647), and it also contains a small amount of ZrO_2 impurities. The result is the same as that reported in the previous literature [30]. Figure 1b shows the XRD patterns of LFP@C and LFP@C/LZO-X (X= 1, 2, 4). The diffraction peaks of the samples with different amounts of LZO are all consistent with the LFP olivine structure (JCPDs PDF# 83-2092), indicating that the introduction of LZO does not affect the phase structure of LFP. And the sharp diffraction peaks also illustrate all the samples are well crystalline. No diffraction peaks of LZO and carbon are observed, which may be due to the small amount of LZO and carbon.
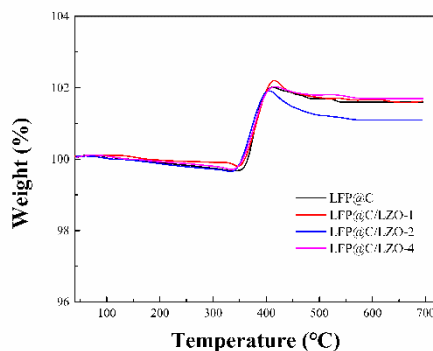

Figure 1. (a) XRD and SEM images of LZO; (b) XRD patterns of as-prepared LFP@C and LFP@C/LZO-X (1, 2, 4)

To measure the carbon content in samples, TG curves were measured. The results are shown in Figure 2. A small amount of weight loss (0.1-0.3 wt%) occurs below 350°C, which is mainly due to the evaporation of the adsorbed water in the samples. Then the samples have a weight gain between 350°C and 430°C, mainly due to the oxidation of $LiFePO_4$ to $Li_3Fe_2(PO_4)_3$ and Fe_2O_3, while the subsequent weight loss can be mainly attributed to the oxidation of carbon. The main mechanism of this process is shown in formula (1). When the temperature reaches 550°C, the weights of the samples remain unchanged and the carbon has been completely oxidized. Because of the oxidation of carbon, the weight gains of the final samples are lower than the theoretical increase of 5.07 wt% of pure LFP [31], so the carbon content can be calculated by the difference between them, as shown in formula (2):
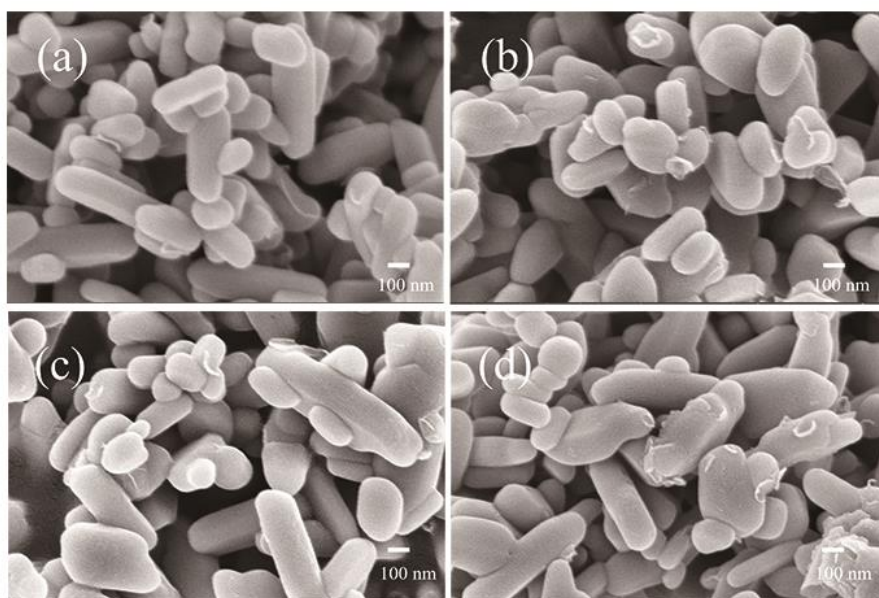
$$LiFePO_4 + nC + (n + \frac{1}{4})O_2 \rightarrow \frac{1}{3}Li_3Fe_2(PO_4)_3 + \frac{1}{6}Fe_2O_3 + nCO_2 \qquad (1)$$

$$x(wt\%) = 5.07 - (A - 1) \qquad\qquad (2)$$

In formula (2), x is the carbon content (wt%) of the final products, and A is the mass percentage of the final products. After calculation, the carbon contents of LFP@C and LFP@C/LZO-X (X = 1, 2, 4) are 3.47 wt%, 3.47 wt%, 3.97 wt%, and 3.37 wt%, respectively.
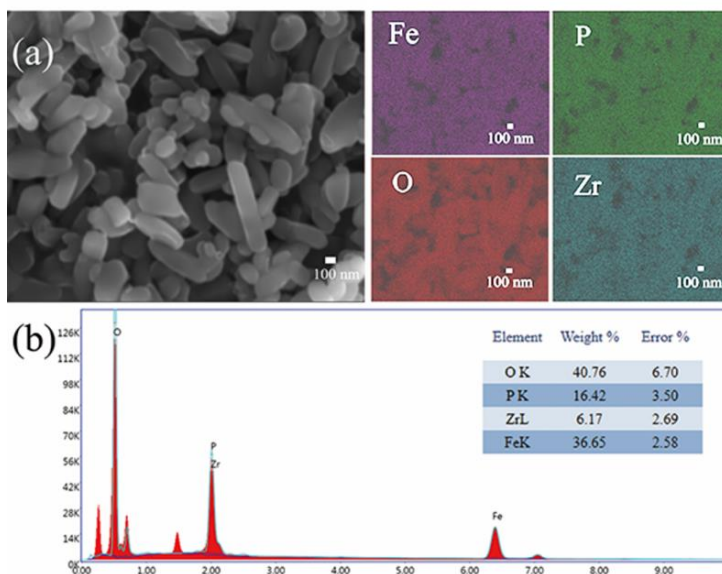

Figure 2. TG curves of as-prepared LFP@C and LFP@C/LZO-X (1, 2, 4).

Figure 3. SEM images of pristine LFP@C(a), LFP@C/LZO-1(b), LFP@C/LZO-2(c), LFP@C/LZO-4(d).

SEM was investigated to study the morphology of the LFP@C/LZO. It can be found that all samples consist of irregular rod-like particles, which are about 200-800 nm in length and 100-200 nm in width. The addition of LZO has little effect on the particle size and the shape of the material, which may be due to the ex-situ addition of LZO. It can also be observed that conductive carbon exists on the particle surface as well as between the particles, and this structure enhances the connection between the particles, which promotes the rapid migration of lithium ions and the formation of electronically conductive networks. Figure 4a shows the element mapping images of LFP@C/LZO-2. It can be found that Fe, P,

Zr, and O are all uniformly distributed on the sample, proving that LZO exists on the LFP surface. Figure 4b presents the EDS image of LFP@C/LZO-2. According to the semi-quantitative results, the mass ratio of Fe: Zr can be calculated to be 5.94, which is close to the theoretical value of 6.79, which also indicates that Zr has been successfully doped into LFP@C.
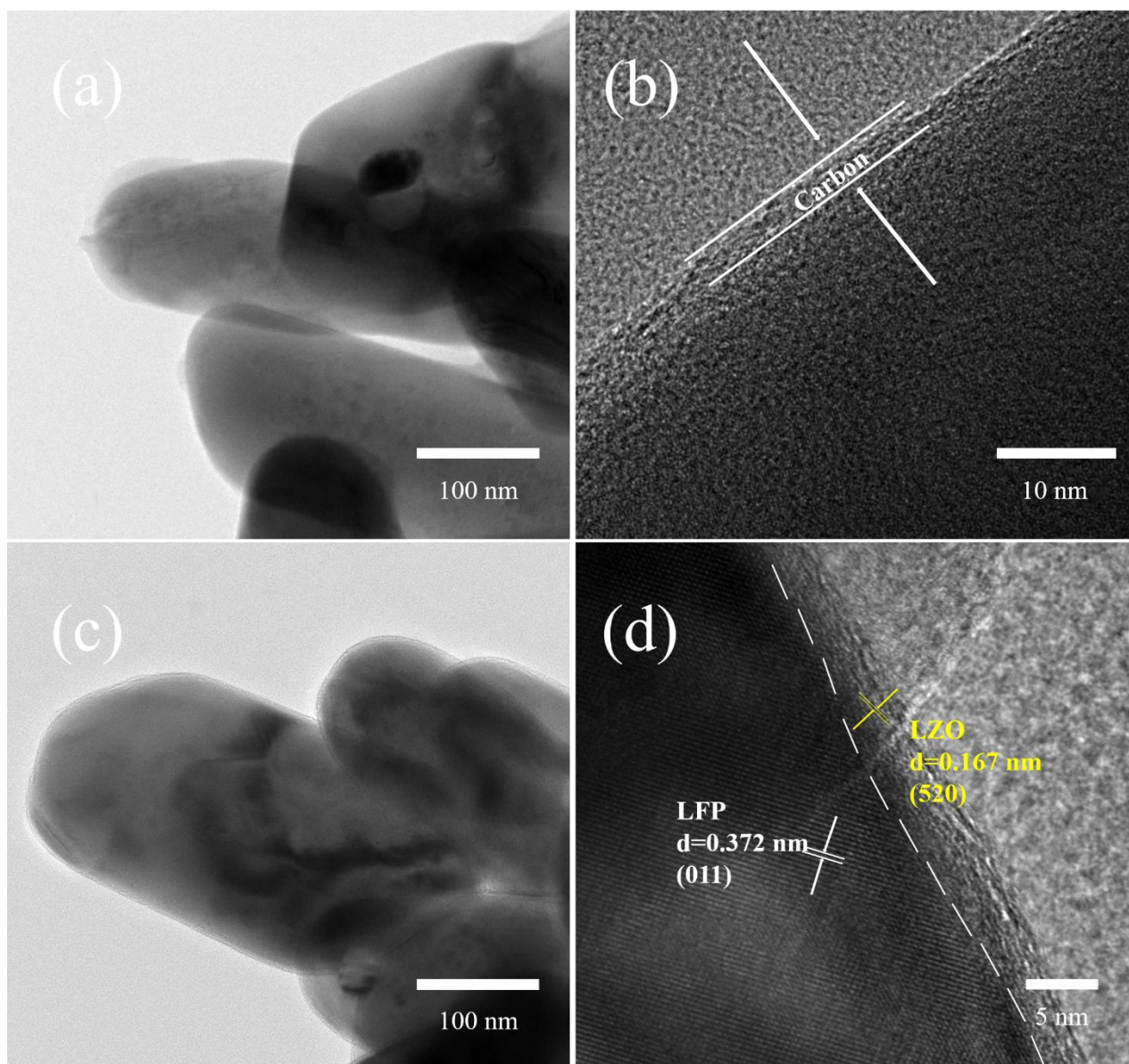

Figure 4. The elemental mapping images (a) and EDS image (b) of LFP@C/LZO-2.

TEM was used to further study the surface coating of LFP. Figure 5d shows the HRTEM of LFP@C/LZO-2. The lattice spacing of 0.372 nm can be well matched to the (011) plane of LFP, while the lattice spacing of 0.167 nm is perfectly matched to the (520) plane of LZO. Besides, only the carbon layer-coated LFP can be observed on the upper right side, so the coating of LZO may be uneven. The coating of LZO is beneficial to promote the transfer of surface charge [21] and avoid direct contact of HF with the electrode material.
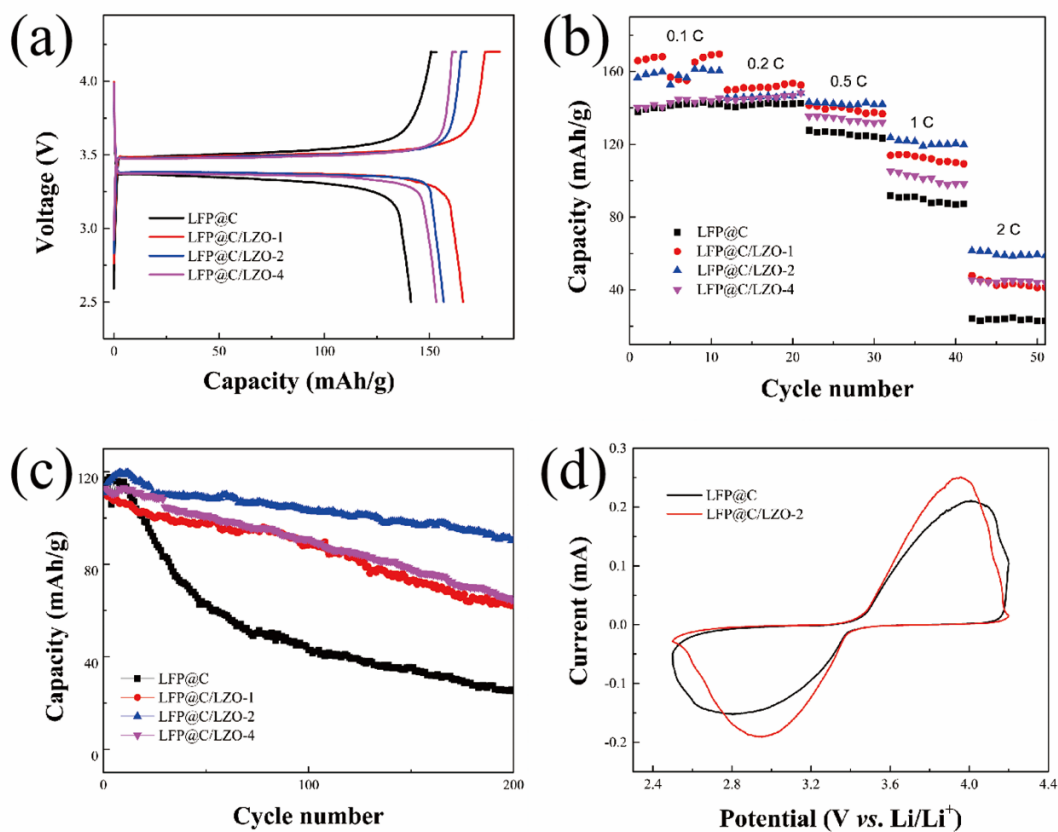
All samples were evaluated by charge-discharge tests at 0.1 C and the obtained results were presented in Figure 6a. All electrode materials display a flat and stable voltage platform between 3.4 V and 3.5 V, demonstrating that the addition of Li_2ZrO_3 did not change the phase transfer of lithium iron phosphate during charge and discharge [32-34]. When the coating amount is 0, 1, 2, 4 wt%, the capacities of the samples at 0.1 C are 141.2 mAh/g, 165.9 mAh/g, 156.7 mAh/g, 153.2 mAh/g, respectively. It can be found that compared with the uncoated sample, the initial discharge capacities of the LFP@C/LZO have been improved greatly, and when the coating amount is 1 wt%, the LFP@C/LZO-1 delivers the best electrochemical properties. Further increasing the coating amounts, the initial discharge capacities of the samples decrease. This is because a small content of LZO can decrease polarization and side effects. However, it is an electrochemically inert substance [35], excess contents will inevitably reduce the proportion of active material and eventually affect the capacity of the material.

Figure 5. TEM and HRTEM images of LFP@C (a, b) and LFP@C/LZO-2 (c, d).

As is presented in Figure 6b, the materials with coating amounts of 1 wt% and 2 wt% possess excellent electrochemical performance compared to the uncoated and 4 wt% samples. The discharge capacity of the LFP@C/LZO-1 is superior at a low rate, which is identical to the previous results in Figure 6a. When the discharge rate is changed to 0.5 C and above, LFP@C/LZO-2 with a coating amount of 2 wt% shows better rate performance and can maintain 61 mAh/g even at 2 C. This may be because the LZO content of 1 wt% is too small and cannot protect the cathode material at a higher current density. This also shows that the addition of an appropriate amount of Li_2ZrO_3 can elevate the lithium-ion diffusion rate and improve rate capacity.

Figure 6. (a) The initial charge and discharge profiles of LFP@C and LFP@C/LZO-X (1, 2, 4); (b) rate performances of LFP@C and LFP@C/LZO-X (1, 2, 4); (c) cycling performances of LFP@C and LFP@C/LZO-X (1, 2, 4) at 1 C; (d) CV curves of LFP@C and LFP@C/LZO-2.

Figure 6c presents the cycle performance of LFP@C/LZO at 1 C. LFP@C/LZO-2 with 2 wt% Li_2ZrO_3 delivers an initial discharge capacity of 111 mAh/g at 1 C and remarkable cycle performance which it can retain 90.6 mAh/g after 200 cycles and the retention rate is 81.62%. And it can be seen that the cyclic stability of LFP@C/LZO-2 is much better than other samples. The increased capacity retention may be because Li_2ZrO_3 weakens the dissolution of lithium iron phosphate by HF from the electrolyte [36] and enhances the stability of the material. This electrochemical performance is better than most of the LFPs listed in Table 1, but its rate performance still needs further improvement. Figure 6d shows the CV curves of LFP@C and LFP@C/LZO-2 in the voltage window of 2.5-4.2 V. The two redox peaks are mainly for the Fe^{2+}/Fe^{3+} redox couple. And compared with LFP@C, the narrower peak separation and higher symmetry of LFP@C/LZO-2 indicate that the material has smaller polarization and higher electrochemical reversibility, while the higher peak current denotes that it has a faster lithium-ion diffusion rate [37]. Such changes are mainly because LZO can reduce the polarization between materials and improve the ionic diffusivity of LFP materials.

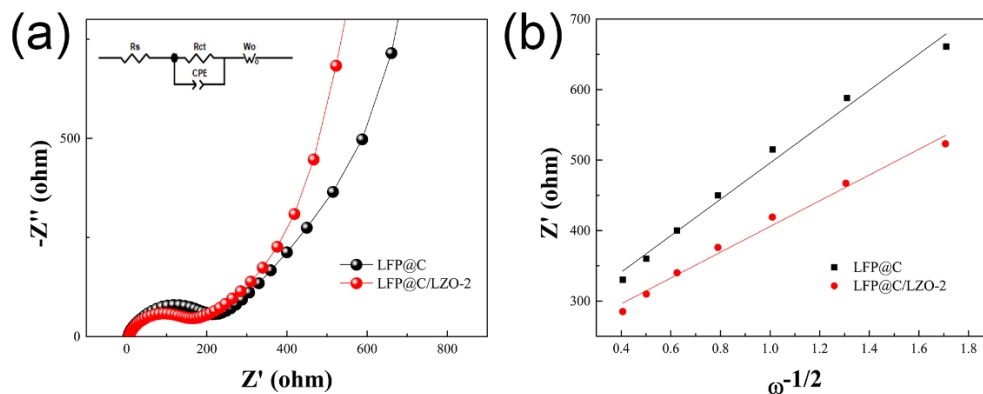**Table 1.** Comparison of electrochemical properties of LFP materials

References	discharge capacities/mAh·g^{-1} (0.1 C)	discharge capacities/mAh·g^{-1} (1 C)
This study	156.7	111
LFP/C-xZnO [38]	138.7	-
HY-SO-LFP [32] consecutive combination of sol-gel and hydrothermal methods	124	109
Al-doped Li$_7$La$_3$Zr$_2$O$_{12}$-LFP [18]	147.5	109.6
LFP-TiO$_2$-C-N [39]	165.3	145.5
LFP/MNC-859 [40]	132.3	119.7

EIS was conducted to better study the influence of LZO on LFP interface impedance. The Nyquist diagram and its equivalent circuit are displayed in Figure 7a. The intercept in the high-frequency area expresses the electrolyte resistance, while the high-frequency semicircle is related to the charge transfer impedance (R_{ct}) which is associated with the electrode reaction. The straight line in the low frequency zone refers to the lithium-ion diffusion in the active materials [41-43]. The charge transfer impedances of LFP@C and LFP@/LZO-2 are 173.7 Ω and 132.9 Ω, respectively; and the lithium-ion migration rate (D_{Li^+}) can be obtained using the formula listed below [44]:

$$D_{Li^+} = \frac{R^2 T^2}{2A^2 n^4 F^4 C^2 \sigma^2} \qquad (3)$$

$$Z' = R_s + R_{ct} + \sigma\omega^{-\frac{1}{2}} \qquad (4)$$

Here, R represents the gas constant (8.314 J/(K·mol), T denotes the temperature (298.15 K), A means the electrode area (1.5386 cm^2), n is the number of electrons in the electrode reaction (n=1), F and C are the Faraday constant (96500 C/mol) and the lithium-ion concentration (3.966×10^{-3} mol/cm^3), respectively. σ represents the Warburg factor (Ω·s^{-1}), which can be obtained by formula (4). The calculated D_{Li^+} of LFP@C and LFP@C/LZO-2 are 1.4285×10^{-14} and 2.8489×10^{-14} cm^2/s, respectively. In summary, coating LZO on the surface of LFP can indeed increase the lithium-ion diffusion rate.

Figure 7. (a) EIS of LFP@C and LFP@C/LZO-2 and the corresponding equivalent circuit; (b) The fit plot of Z' vs. $\omega^{-1/2}$

4. CONCLUSIONS

In short, we successfully synthesized Li_2ZrO_3 coated lithium iron phosphate, and studied the influences of different contents (0, 1, 2, 4 wt%) on the material. The results show that the addition of Li_2ZrO_3 has no significant effect on the morphology of the material. And when the coating amount is 2 wt%, LFP@C/LZO-2 shows the best rate performance (61 mAh/g / 2 C) and excellent cycle performance (81.62% / 200th). The significant improvement may be due to the fact that Li_2ZrO_3 and carbon jointly construct a cross-linked conductive network of lithium iron phosphate and act as a surface sacrificial agent to weaken the damage of HF generated by the electrolyte to the active material. The research has enriched the selection range of lithium iron phosphate coating materials and also provides a new option for other cathode materials.

References

1. Y.B. Guan, J.R. Shen, X.F. Wei, Q.Z. Zhu, X.H. Zheng, S.Q. Zhou and B. Xu, *Electrochim. Acta,* 294 (2019) 148.
2. S.Y. Ju, T. Liu, H.R. Peng, G.C. Li and K.Z. Chen, *Mater. Lett.,* 93 (2013) 194.
3. X.D. Zhang, Z.Y. Bi, W. He, G. Yang, H. Liu and Y.Z. Yue, *Energy Environ. Sci.,* 7 (2014) 2285.
4. B. Wang, Y. Xie, T. Liu, H. Luo, B. Wang, C.H. Wang, L. Wang, D.L. Wang, S.X. Dou and Y. Zhou, *Nano Energy,* 42 (2017) 363.
5. C. Delacourt, P. Poizot, S. Levasseur and C. Masquelier, *Electrochem. Solid-State Lett.,* 9 (2006) A352.
6. Y. Liu, Y.J. Gu, G.Y. Luo, Z.L. Chen, F.Z. Wu, X.Y. Dai, Y. Mai and J.Q. Li, *Ceram. Int.,* 46 (2020) 14857.
7. Z.X. Yan, D.Q. Huang, A.J. Lai, Y.Q. Chu, F.H. Zheng, Y.Z. Cai, Q.C. Pan, H.Q. Wang, Y.G. Huang and Q.Y. Li, *Electrochim. Acta,* 353 (2020) 136565.

8. H.Q. Wang, A.J. Lai, D.Q. Huang, Y.Q. Chu, S.J. Hu, Q.C. Pan, Z.H. Liu, F.H. Zheng, Y.G. Huang and Q.Y. Li, *New J. Chem.,* 45 (2021) 5695.
9. Y. Li, L. Wang, F. Liang, Y.C. Yao and K.Y. Zhang, *J. Alloys Compd.,* 880 (2021) 160560.
10. X. Chu, L.M. Li, W. Chen and H.S. Fang, *Ionics,* 27 (2021) 2927.
11. S.N. Zhao, L. Wen, J.L. Liu, J.Q. Chen and F.L. Bei, *Int. J. Electrochem. Sci.,* (2020) 8873.
12. Y. Liu, W.C. Qin, D.K. Zhang, L.W. Feng and L. Wu, *Prog. Nat. Sci.: Mater. Int.,* 31 (2021) 14.
13. X.M. Cui, D.W. Yi, N.L. Li, L. Zhang, X.F. Zhang and D.Y. Yang, *Energy Fuels,* 34 (2020) 7600.
14. D.W. Yi, X.M. Cui, N.L. Li, L. Zhang and D.Y. Yang, *ACS Omega,* 5 (2020) 9752.
15. X.F. Wang, Z.J. Feng, X.L. Hou, L.L. Liu, M. He, X.S. He, J.T. Huang and Z.H. Wen, *Chem. Eng. J.,* 379 (2020) 122371.
16. H.W. Zhang, J.Y. Li, L.Q. Luo, J. Zhao, J.Y. He, X.X. Zhao, H. Liu, Y.B. Qin, F.Y. Wang and J.J. Song, *J. Alloys Compd.,* 876 (2021) 160210.
17. M. Shi, R.W. Li and Y.L. Liu, *J. Alloys Compd.,* 854 (2021) 157162.
18. Y.X. Bai, J. Zhang, Y.B. Yang, R. Yang, Y.L. Yan and J. Wang, *J. Alloys Compd.,* 843 (2020) 154915.
19. L.X. Yuan, Z.H. Wang, W.X. Zhang, X.L. Hu, J.T. Chen, Y.H. Huang and J.B. Goodenough, *Energy Environ. Sci.,* 4 (2011) 269.
20. S.X. Zhao, H. Ding, Y.C. Wang, B.H. Li and C.W. Nan, *J. Alloys Compd.,* 566 (2013) 206.
21. J.W. Zhao, S.X. Zhao, X. Wu, H.M. Cheng and C.W. Nan, *J. Alloys Compd.,* 699 (2017) 849.
22. Z.P. Ma, G.J. Shao, X.J. Qin, Y.Q. Pan, G.L. Wang, J.J. Song and T.T. Liu, *J. Power Sources,* 269 (2014) 194.
23. C.C. Yang, J.R. Jiang, C. Karuppiah, J.H. Jang, Z.H. Wu, R. Jose and S.J. Lue, *J. Alloys Compd.,* 765 (2018) 800.
24. Z.P. Ma, Y.S. Peng, G.L. Wang, Y.Q. Fan, J.J. Song, T.T. Liu, X.J. Qin and G.J. Shao, *Electrochim. Acta,* 156 (2015) 77.
25. G.R. Hu, P.W. Chen, Y.B. Cao, Z.D. Peng, D. Ke and Z.J. Zhang, *Solid State Ionics,* 301 (2017) 138.
26. J.N. Zhang, G. Sun, Y. Han, F.D. Yu, X.J. Qin, G.J. Shao and Z.B. Wang, *Electrochim. Acta,* 343 (2020) 136105.
27. J.C. Zhang, R. Gao, L.M. Sun, H. Zhang, Z.B. Hu and X.F. Liu, *Electrochim. Acta,* 209 (2016) 102.
28. J.P. Han, B. Zhang, X. Bai, L.Y. Wang, Y.X. Qi, N. Lun and Y.J. Bai, *J. Power Sources,* 354 (2017) 16.
29. D. Wang, X.H. Li, W.L. Wang, Z.X. Wang, H.J. Guo and J.J. Ru, *Ceram. Int.,* 41 (2015) 6663.
30. L.M. Zhu, L.L. Mo, L.L. Xie and X.Y. Cao, *Electrochem. Commun.,* 122 (2021) 106908.
31. S.L. Yang, M.J. Hu, L.J. Xi, R.G. Ma, Y.C. Dong and C.Y. Chung, *ACS Appl. Mater. Interfaces,* 5 (2013) 8961.
32. M.A.M.M. Alsamet and E. Burgaz, *Electrochim. Acta,* 367 (2021) 137530.
33. C.Z. Li, H.Y. Yuan and Z.J. Yang, *Solid State Ionics,* 352 (2020) 115366.
34. H.G. Deng, S.L. Jin, L. Zhan, Y.L. Wang, W.M. Qiao and L.C. Ling, *J. Power Sources,* 220 (2012) 342.
35. S.T. Sun, C.Q. Du, D.Y. Qu, X.H. Zhang and Z.Y. Tang, *Ionics,* 21 (2015) 2091.
36. X.W. Miao, H. Ni, H. Zhang, C.G. Wang, J.H. Fang and G. Yang, *J. Power Sources,* 264 (2014) 147.
37. X.F. Wang, Z.J. Feng, J.T. Huang, W. Deng, X.B. Li, H.S. Zhang and Z.H. Wen, *Carbon,* 127 (2018) 149.
38. X.H. Chen, Y. Li and J. Wang, *nanomaterials,* 11 (2021) 12.
39. J.Y. Shi, X.Q. Zhang, X.K. Zhang and Y. Xiang, *J. Alloys Compd.,* 750 (2018) 139.
40. S. Khan, R.P. Raj, T.V.R. Mohan and P. Selvam, *RSC Adv,* 10 (2020) 30406.
41. Y. Li, L. Wang, K.Y. Zhang, F. Liang, M.M. Yuan, H. Zhang and Y.C. Yao, *Vacuum,* 184 (2021)

  109935.
42. G.Y. Luo, Y.J. Gu, Y. Liu, Z.L. Chen, Y.L. Huo, F.Z. Wu, Y. Mai, X.Y. Dai and Y. Deng, *Ceram. Int.,* 47 (2021) 11332.
43. Y. Wang, J.P. Zhang, S.Y. Tian, J.J. Xue, L.Z. Wen and G.C. Liang, *Ionics,* 27 (2021) 993-1002.
44. Y.H. Zou, G.J. Chang, S. Chen, T.C. Liu, Y.Z. Xia, C.M. Chen and D.J. Yang, *Chem. Eng. J.,* 351 (2018) 340.